DIP/Dpr interactions and the evolutionary design of specificity in protein families

Alina P. Sergeeva, Phinikoula S. Katsamba, Filip Cosmanescu, Joshua J. Brewer, Goran Ahlsen, Seetha Mannepalli, Lawrence Shapiro, Barry Honig

Affiliations

Department of Biochemistry and Molecular Biophysics, Columbia University, New York, NY, USA

Alina P. Sergeeva, Phinikoula S. Katsamba, Filip Cosmanescu, Joshua J. Brewer, Goran Ahlsen, Seetha Mannepalli, Lawrence Shapiro, Barry Honig

Zuckerman Mind, Brain and Behavior Institute, Columbia University, New York, NY, USA

Alina P. Sergeeva, Phinikoula S. Katsamba, Filip Cosmanescu, Joshua J. Brewer, Goran Ahlsen, Seetha Mannepalli, Lawrence Shapiro, Barry Honig

Department of Systems Biology, Columbia University, New York, NY, USA

Alina P. Sergeeva, Lawrence Shapiro, Barry Honig

Department of Medicine, Columbia University, New York, NY, USA

Barry Honig

Abstract

Differential binding affinities among closely related protein family members underlie many biological phenomena, including cell-cell recognition. *Drosophila* DIP and Dpr proteins mediate neuronal targeting in the fly through highly specific protein-protein interactions. DIPs/Dprs segregate into seven specificity subgroups defined by binding preferences between their DIP and Dpr members. Here we describe a novel sequence-, structure- and energy-based computational approach, combined with experimental binding affinity measurements, to reveal how specificity is coded on the canonical DIP/Dpr interface. We show that binding specificity of DIP/Dpr subgroups is controlled by

"negative constraints", which interfere with binding. To achieve specificity, each subgroup utilizes a different combination of negative constraints, which are broadly distributed and cover the majority of the protein-protein interface. We discuss the structural origins of negative constraints, and potential general implications for the evolutionary origins of binding specificity in multi-protein families.

Introduction

Over the course of evolution, gene duplications followed by sequence divergence have generated numerous protein families whose homologous members have distinct binding specificities. In many cases there are only subtle differences in the sequence and structure of closely related family members, yet these can have profound functional consequences. Families of cell-cell adhesion proteins offer many such examples where seemingly small changes in sequence generate new specificities for protein-protein interaction specificities. For example, invertebrate Dscam[1,2] and vertebrate clustered protocadherin[3,4] neuronal "barcoding" proteins each display strict intra-family homophilic specificity. While one Dscam (or Pcdh) isoform may have >90% sequence identity to another family member, the few differences between isoforms selected by nature ensure that only homophilic recognition occurs; this is critical to their mechanism of function in diversification of neuronal identities and self/non-self-discrimination. In other cases, for example the type I and type II classical cadherins[5-7], which pattern epithelia and other tissue structures, specificity is less strict. While classical cadherins also exhibit homophilic binding, in addition they show strong heterophilic binding to other select family members. In another example, the nectin[8] adhesion protein family encodes interactions between members that are mainly heterophilic, in some cases to form a checkerboard pattern between two cell types, each expressing a cognate nectin. The specificity patterns of these protein families underlie their biological functions, and are conserved in evolution. Understanding how specificity is coded on multi-protein adhesion protein families is thus critical.

Here we carry out a comprehensive computational and experimental study of specificity determinants in two interacting families of neuronal recognition proteins, the 21-member Dpr

(Defective proboscis extension response) and the 11-member DIP (Dpr Interacting Proteins). These proteins have been extensively characterized structurally[9-11], and their interactions were characterized quantitatively with biophysical measurements[11], thus offering an ideal system to study the evolutionary design of specificity on protein-protein interfaces. DIPs and Dprs are expressed in cell-specific patterns throughout the developing nervous system[12]. DIPs preferentially bind Dprs, and a network of specific heterophilic interactions is formed between members of the two families. This molecular binding network is correlated with synaptic specificity in the fly retina, suggesting that DIP/Dpr interactions play an important role in neuronal patterning[9,13].

The extracellular regions of DIP and Dpr family members consist of three and two tandem Ig-like domains, respectively[13]. Homodimerization is observed for some DIPs and Dprs, and homo- and hetero-dimerization is mediated by an interface formed between the membrane-distal Ig1 domains (Figure 1A). Surface plasmon resonance (SPR) showed that members of both families have distinct binding profiles, with DIPs and Dprs initially classified as forming four specificity subgroups.[11] In the current work we extended the number of subgroups to seven based primarily on the strongest heterophilic binding preferences but also on DIP/Dpr sequence similarity (see color-coded subgroup assignment in Figure 1B). Our DIP/Dpr grouping is somewhat different than that published by Cheng et al.[10] due in part to the fact that these authors did not include DIP-κ and DIP-λ, whose binding preferences had been previously mapped[11]. Additional differences could be due to the biophysical approaches used to measure DIP/Dpr binding affinities in Cosmanescu et al.[11] and Cheng et al.[10] (see methods).

The Ig1 domains of the *Drosophila Melanogaster* DIPs and Dprs have intra-family pairwise sequence identities greater than about 50% and 40%, respectively, while the average identity between individual DIPs and Dprs is about 30%. Binding interfaces for crystallographically determined hetero-dimer structures are essentially identical – superimposing to within 1Å (Figure 1C)[11]. The central question we address here is how DIPs and Dprs that are so closely related in sequence and structure can exhibit such highly specific pairwise interactions. Previous studies have

identified specificity residues for select DIP/Dpr interactions[9-11]. Here, we analyze specificity for the family as a whole. Our results reveal the central role of "negative constraints" - destabilizing interfacial positions, which preclude complex formation between members of some specificity groups, while allowing it between others. We use the term negative constraints here to denote an amino acid in a cognate interface that interferes with binding to a non-cognate partner. The term negative constraint has been used in the field of protein design[14-17] to denote a domain that must be designed against, in effect an "anti-target". In contrast, our use of the term here focuses on individual amino acids rather than entire domains.

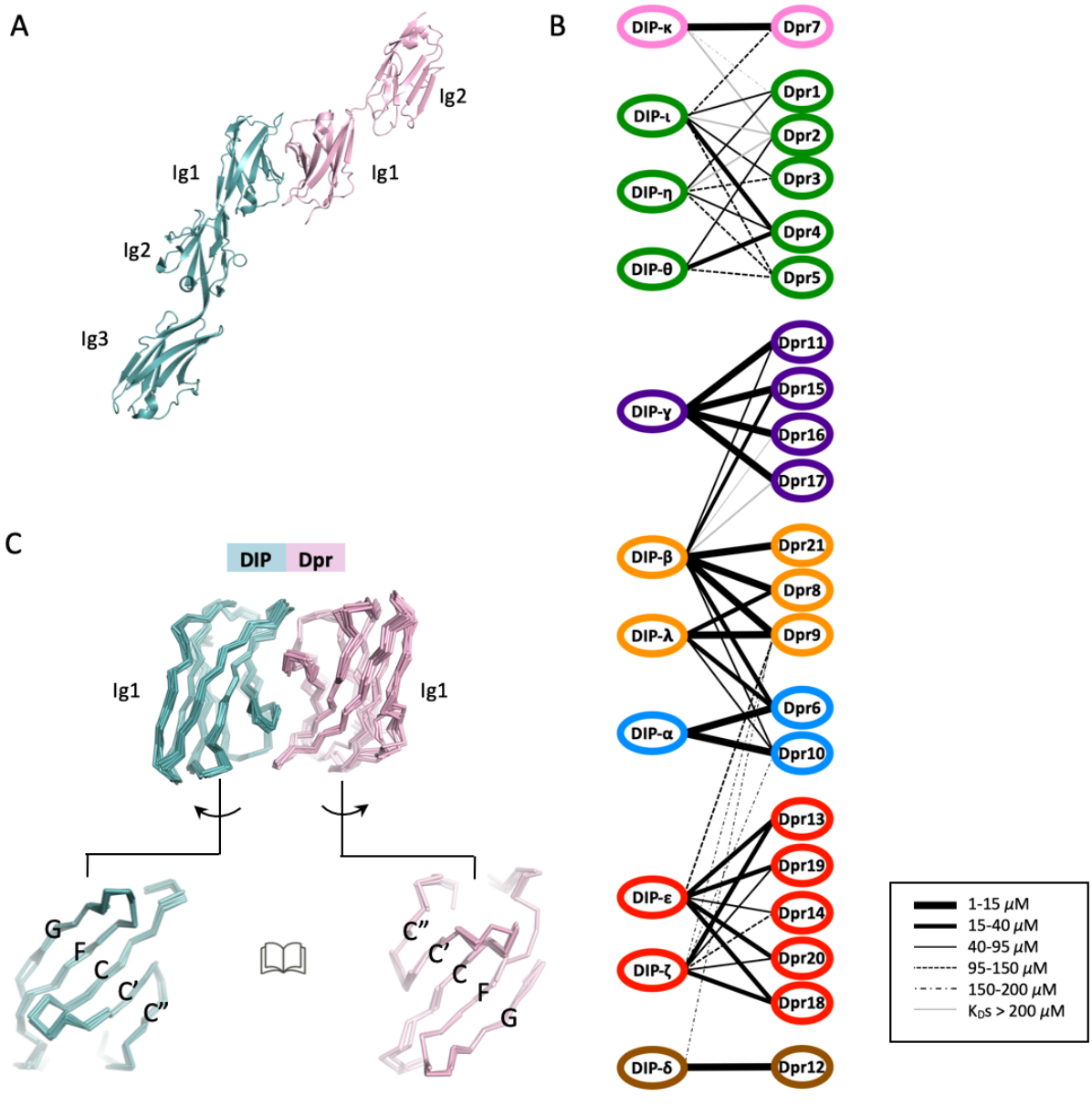

Figure 1. Structure and interaction properties of DIPs and Dprs. (A) Ribbon representation of the DIP/Dpr heterodimer (PDBID: 6EG0)[11] – DIP shown in cyan, Dpr in pink. **(B)** Affinity-based binding interactome of DIPs and Dprs of *Drosophila Melanogaster*. Line thickness indicates the K_D for a given pairwise interaction, as specified in the boxed inset. Groupings are color-coded based on their heterophilic binding preference. The interactome is based on previously published SPR data[11]. **(C)** Structural alignment of Ig1 domains in DIP/Dpr complexes (see Methods for PDBIDs). DIPs and Dprs interact via their CC'C"FG surfaces.

Since there are a total of forty-nine possible DIP/Dpr subfamily pairs and only seven bind strongly, there must be forty-two sets of negative constraints that preclude incorrect pairing. These are coded on a pseudo-symmetric Ig1'-Ig1" interface of about 1900 Å^2 buried surface area and comprising 33 interfacial residues on the DIP side and 33 interfacial residues on the Dpr side. We

recognize that non-interfacial residues may also contribute to specificity but the primary determinants will, in most cases, be part of the interface and these are the focus of the current work.

We begin by asking what can be learned from sequence alone and find that the information available is useful but incomplete. Our structure-based approach involves building homology models of hypothetical complexes formed between all DIPs and Dprs and, also using solved complexes where available, to calculate the energetic consequences of mutating interfacial residues in one family member to those of every other. We tested various programs that calculate binding free energy changes ($\Delta\Delta$Gs) resulting from mutations and found that FoldX[18] offered the best combination of accuracy and computational efficiency. Using FoldX, we identified negative constraints for every DIP/Dpr pair and then confirmed a subset of our predictions using quantitative biophysical assays (AUC and SPR).

Our results provide a detailed account of the design of complex specificity on a canonical protein-protein interface. Most of the interface is used to create negative constraints with virtually all expected energetic terms (steric hindrance, Coulombic repulsion, unsatisfied buried charges and/or polar groups) used to weaken undesired complex formation between different subgroup pairs. Some locations on the interface are used by multiple pairs while others are used in only a small number of cases. In general, more than one negative constraint is required to significantly weaken binding. We also discuss the trade-off between specificity and affinity, a phenomenon that appears essential for the generation of multiple specificity groups[14,15,19]. Overall, our analysis reveals general principles about the design of protein families whose members are very similar in sequence and structure and yet exhibit exquisitely controlled binding affinities and specificities.

Results

Sequence analysis of DIPs and Dprs

Figure 2 plots an alignment of sequence logos corresponding to interfacial residues of DIP and Dpr *Insecta* orthologs (see Methods for details). Interfacial positions of DIPs and Dprs were

assigned based on non-zero change in accessible surface area per residue upon complex formation in experimentally solved crystal structures. Interfacial positions of DIP/Dpr complexes of unknown structure were inferred from multiple sequence alignment (residue correspondence with interfacial positions of solved complexes). The family-wide numbering of interfacial positions (*i* = 1-33, designated above the logos in Figure 2) is used throughout the paper (see correspondence between the family-wide numbering and Uniprot numbering (given throughout this paper in curly brackets) in Table S1).

Four positions shown in yellow are occupied almost exclusively by hydrophobic residues which form the hydrophobic core of the DIP/Dpr interface[10] (Figure 2A). Additionally, shown in purple is a conserved Gln in both subfamilies and a conserved Asn in DIPs, which interlock the Ig1'-Ig1" interface by forming buried sidechain-to-backbone hydrogen bonds (Figure 2B). Residues that are conserved across subfamilies cannot be responsible for subgroup specificity but changes in the identity of individual conserved hydrophobic residues can play a role (see below). Rather, potential specificity determinants will generally correspond to positions that are conserved in at least one subfamily but differ in between subfamilies.

We tested the ability of a number of sequence-based methods to identify specificity determinants in the seven specificity subgroups. These include GroupSim[20], SDPpred[21], SPEER[22] and Multi-Harmony[23].

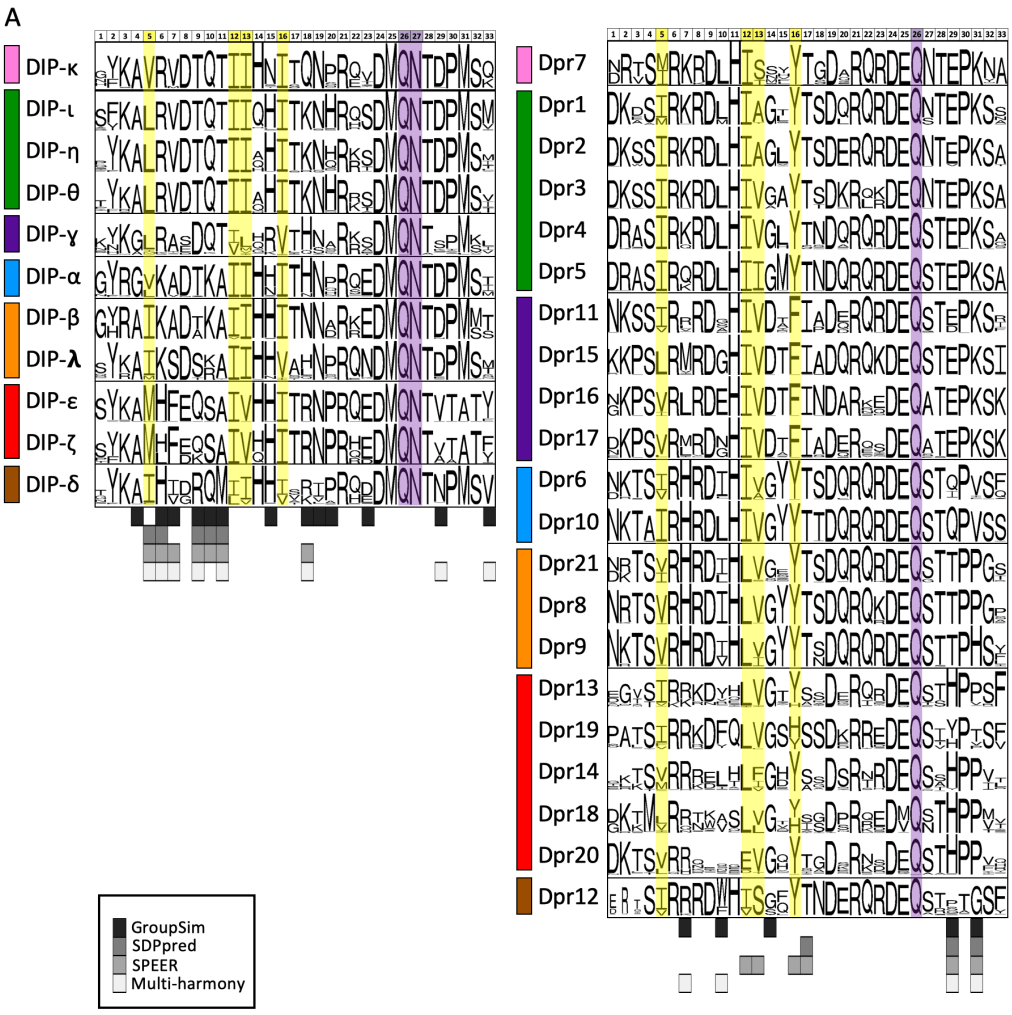

Figure 2. Sequence-based predictions of DIP/Dpr specificity residues and common binding determinants. (A) Alignment of sequence logos corresponding to interfacial residues of DIP and Dpr Insecta orthologs. Predictions of specificity determining positions using sequence-based methods (GroupSim, SDPpred, SPEER, and Multi-Harmony) are given below logos in different shades of grey as specified in boxed inset. Bar on the left of logos indicates color of the DIP/Dpr subgroup (Figure 1B). Family-wide numbering of interfacial positions is given above the alignment. The correspondence between protein specific (UniProt) and family-wide numbering is given in Table S1. See Methods for details on sequence logo preparation. **(B)** Common binding determinants of DIP/Dpr dimers depicted on ribbon Ig1'-Ig1" interfaces in sticks. Hydrophobic interfacial residues are in yellow. Conserved buried hydrogen bonds are depicted by dotted lines. Interfacial positions enclosed in boxes follow family-wide numbering and are annotated with identities of conserved amino-acids.

As input, we used a multiple sequence alignment of just interfacial residues with protein sequences of 1732 DIP or 2570 Dpr orthologs segregated into seven specificity subgroups (see Figure 2 and methods for details). Nine specificity determining positions were identified based on a consensus of at least 3 out of 4 of these methods, and 14 additional positions, were predicted by at least one method (see predictions below logos in grey, Figure 2). These expand the number of predicted specificity determining sites compared to our previous study[11] where we relied on visual inspection of a multiple sequence alignment of DIP/Dpr sequences in *Drosophila* Melanogaster alone. Below we compare the predictions of these sequence-based methods to an energy-based analysis of DIP and Dpr structures.

Identifying negative constraints

We hypothesized that negative constraints are the essential factor that defines DIP/Dpr subgroups and developed a computational strategy to identify and characterize these putative constraints. Since each subgroup (e.g. *i* and *j*) has both DIP and Dpr members, for purposes of discussion we can define four sets of proteins, DIP-*i*, DIP-*j*, Dpr*i* and Dpr*j*. We need to explain why members of set DIP-*i* don't bind to members of set Dpr*j* and, in turn, why members of set DIP-*j* don't bind to members of set Dpr*i*. Since Dpr*i* binds to DIP-*i* while Dpr*j* does not, we first use FoldX calculations to identify residues of Dpr*i* that weaken binding to DIP-*i* when mutated into a residue of Dpr*j*. Thus, we identify negative constraints of Dpr*j* by studying their predicted effects on the binding of mutated Dpr*i* to DIP-*i*. The experimental tests follow the same logic: the K_Ds of mutant Dpr*i* binding to DIP-*i* are used to validate predicted negative constraints on Dpr*j*.

The overall procedure was to start with one or more structures of DIP/Dpr complexes for each subgroup (the template complex) and; 1) to mutate every interfacial residue in the DIP protomer to all residues appearing at the same position in DIPs of other specificity subgroups and then 2) calculate $\Delta\Delta$Gs for the binding of each DIP to the Dpr in the complex. 3) Repeat the

procedure for the Dpr in the complex and then calculate ΔΔGs for its binding to each DIP. Templates that were used include: *blue subgroup* - crystal structure of Dpr6/DIP-α and two conformations of Dpr10/DIP-α[9,10]; *purple subgroup* – crystal structure of Dpr11/DIP-ɣ[10]; *green subgroup* – crystal structures of Dpr4/DIP-η and for two conformations each for Dpr1/DIP-η and Dpr2/DIP-θ)[10,11]; *pink subgroup* - homology model of Dpr7/DIP-κ; *orange subgroup* - homology model of Dpr8/DIP-β; *brown subgroup* - homology model of Dpr12/DIP-δ; *red subgroup* - homology model of Dpr13/DIP-ε. Overall, we predicted the effects of 3044 mutations of 33 interfacial residues of 13 template complexes on the DIP and Dpr side into residues occurring in DIPs and Dprs of other subfamilies (see a supplementary excel file for the FoldX data). Notably, the results depend heavily on the use of homology models (see Methods for details of how they were constructed).

Negative constraints were defined as positions predicted to cause destabilizing effects for *every* DIP or Dpr fly subgroup member in the context of binding to a member of another Dpr or DIP subgroup, respectively. Our energy-based filter also requires that the effect is destabilizing for every subfamily template complex used in the FoldX calculations (see energy filter in methods for details). In addition, we introduced a second filtering step, whereby we only defined a negative constraint as a position that would also be predicted for other *Insecta* species so as to focus on negative constraints that are evolutionarily conserved. The evolutionary filter is based on the assumption that orthologs in the same subfamily conserve their interaction specificity (see methods for data supporting the assumption). To clarify, the energy-based filter is based on FoldX calculations of structures of fly proteins whereas the evolutionary filter is based on comparison of ortholog sequences of different species of insects. The evolutionary filter involved a qualitative analysis of interfacial residues at corresponding positions of DIP-*i* and DIP-*j (*or Dpr*i* and Dpr*j)* in *Insecta* multiple sequence alignments to see if the identities, size or biophysical properties of amino acids in all members of subfamily "*i*" were different from those of subfamily "*j*" at the predicted position (see evolutionary filter in methods for details).

A subset of our predictions (see below) was tested experimentally. Overall, we identified negative constraints for 42 combinations of non-interacting DIP and Dpr subgroups (see supplemental excel file for all FoldX data).

Evaluation of methods to calculate ΔΔG

We tested six algorithms that calculate binding affinity changes upon mutation of individual residues (ΔΔGs) based on reports of their performance in the literature[24-30]. These include FoldX,[18,31] mCSM,[30] BeAtMusic,[27] MutaBind,[29] Rosetta flex ddG,[24] and BindProfX[32]. FoldX, mCSM, and BeAtMusic require from seconds to few minutes of CPU time per single point mutation, while MutaBind, Rosetta flex ddG, and BindProfX take more than an hour. Our evaluation tests were based on 25 experimental ΔΔG values obtained via SPR or AUC measurements of DIP/Dpr and DIP/DIP dimers. Of these, two were published[11] and twenty-three are new (see Figure S1 for supporting AUC and SPR data). Data on the performance of these methods is summarized in Table S2.

As can be seen in Table S2, FoldX, MutaBind, and Rosetta flex ΔΔG perform best on our dataset as they feature the highest Pearson correlation coefficients (PCC). MutaBind is the best performer but it fails to identify stabilizing mutations (shown in green, Table S2) - a failure of all machine learning methods we tested, which is probably reflective of an overrepresentation of destabilizing mutations in training datasets. In addition, we preferred to use methods based on physics-based force fields since these were easiest to interpret in structural terms. Given its performance in terms of speed and accuracy, we settled on FoldX as a computational guide for the identification of negative constraints.

Negative constraints between blue and purple DIP/Dpr subgroups

We discuss Dpr10/DIP-α(blue subgroup) and Dpr11/DIP-γ (purple subgroup) in detail since these pairwise DIP/Dpr interactions have revealed clear associated phenotypes in the central and

peripheral nervous systems of *Drosophila Melanogaster*[9,33-35]. We consider four sets of negative constraints that weaken blue/purple inter-subgroup DIP/Dpr binding: a) On purple subgroup Dprs; b) On blue subgroup DIP-α; c) On blue subgroup Dprs; and d) On purple subgroup DIP-γ.

a) *Negative constraints on purple subgroup Dprs that weaken binding to blue subgroup DIP-α.* As described in the protocol summarized above, we identify negative constraints on purple Dprs by computationally mutating every interfacial amino acid on blue Dprs to those of purple Dprs and calculating ΔΔGs for binding to DIP-α. This procedure is applied for every template complex listed above. Figure 3A summarizes results using one of the DIP-α/Dpr10 crystal conformations (chains C and D of the asymmetric unit). The figure shows an alignment of the four purple Dprs with blue Dpr10. Each column in the alignment is color-coded based on the ΔΔG for mutating a residue in Dpr10 to the aligned residue in a purple Dpr. Every position where the resulting ΔΔG is positive for all purple Dprs is a candidate for a negative constraint. Predictions are then filtered based on the requirement that ΔΔG >= 0.05 kcal/mol for all available blue subgroup crystal structures (see Figure S2). In addition to the energy filter, only positions that pass evolutionary filter (see above) are accepted.

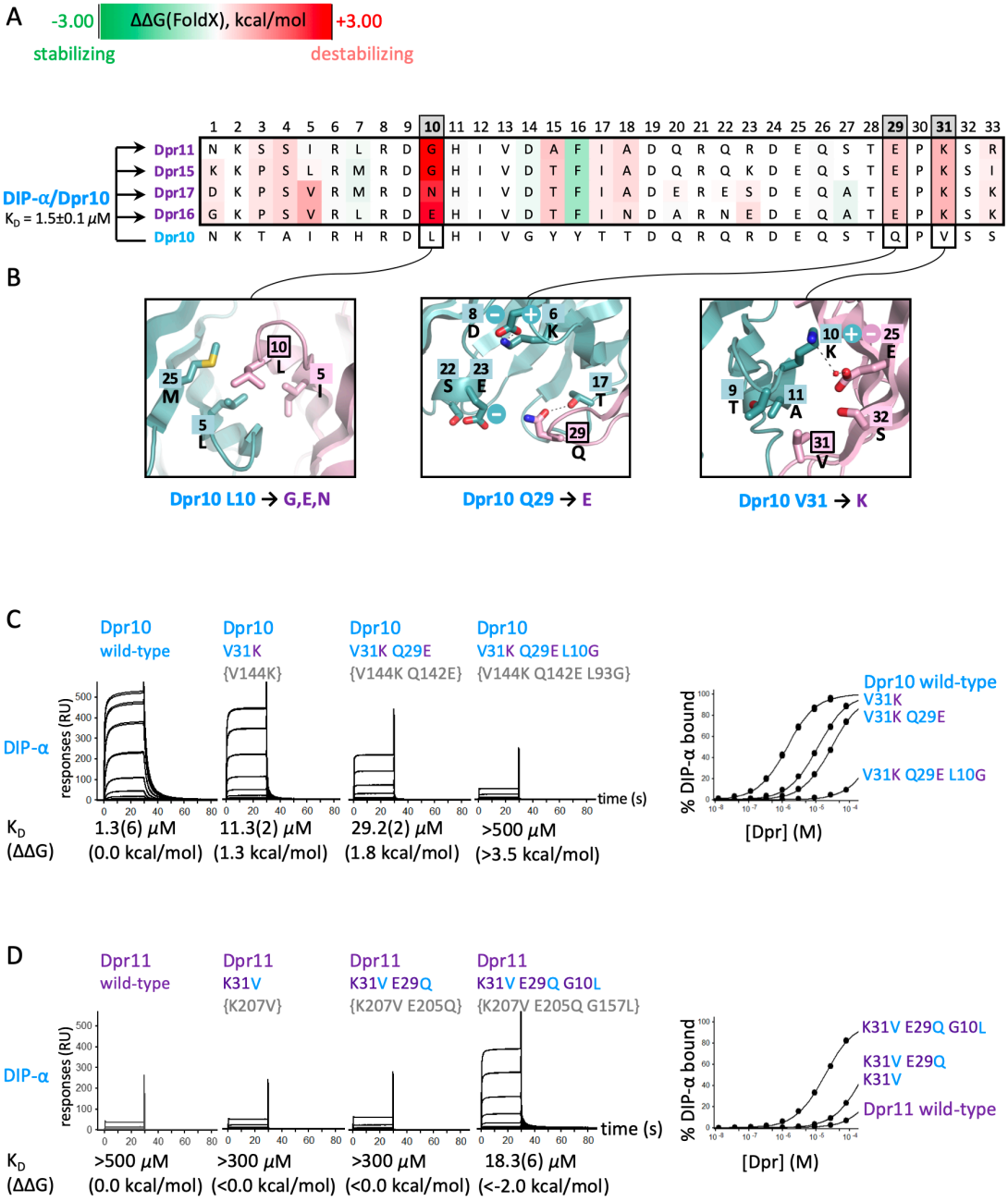

Figure 3. Negative constraints on purple Dprs 11/15/16/17 which prevent binding to the blue DIP-α. (A) Alignment of interfacial residues of the four purple group Dprs and of Dpr10. Residues are color-coded based on the calculated ΔΔG, as specified in the color bar at the top of the figure. Predicted negative constraint positions are in grey. The average K_D for wild-type DIP-α/Dpr10 interaction based on six independent experimental measurements is given on the left of the alignment. All calculations are carried out on the DIP-α/Dpr10 complex indicated to the left of the figure. The arrows indicate that residues in Dpr10 were computationally mutated to those of the four purple Dprs, as indicated. **(B)** Structural details of wild-type environment for each position where a mutation is predicted to cause a negative constraint (enclosed in a bold box). **(C) and (D).** SPR binding analysis of Dpr10 and Dpr11 mutants, representing negative constraints, to DIP-α. Each row shows SPR sensorgrams of Dpr analytes binding over a DIP-α immobilized surface. An overlay of the binding isotherms for each surface is shown to the right. K_D (ΔΔG) values for each DIP/Dpr interaction are listed below the SPR sensorgrams. For each K_D, the number in parenthesis represents the fitting error in the last significant figure, in μM. Family-wide numbering of interfacial positions is used for all the mutants. Uniprot numbering is given in curly brackets.

265 This procedure identified three interfacial positions, 10, 29, and 31 (Figure 3A), as negative
266 constraints. Notably, stabilizing mutations (shown in green) suggest that DIP/Dpr complexes are not
267 fully optimized for binding (see below). The destabilizing effect of these four negative constraints can
268 be understood in biophysical terms (Figure 3B). Dpr10 has a conserved hydrophobic residue at
269 position 10 whose interaction with buried hydrophobic residues of DIP-α contributes favorably to
270 binding (first panel in Figure 3B). When this interaction is lost via mutation to glycine (Dpr11 and
271 Dpr15), a negatively charged glutamate (Dpr16), or a polar asparagine (Dpr17), the DIP/Dpr
272 complexes are destabilized either through the creation of a cavity in the hydrophobic interface or
273 from the desolvation penalty associated with placing charged or polar atoms in the hydrophobic
274 environment. Two other negative constraints correspond to conserved charged Glu and Lys at
275 interfacial positions 29 and 31. These residues form salt bridges in the purple DIP/Dpr subfamily, but
276 would create unsatisfied charges in the context of binding to DIP-α.
277 We tested these predictions with SPR measurements of mutant proteins. Figure 3C displays
278 SPR sensorgrams of Dpr10 wild-type and its mutants passed over a chip immobilized with DIP-α. As
279 can be seen in the figure, the V31K single mutant increases the K_D relative to wild-type by about an
280 order of magnitude; adding a second mutation, Q29E, further increases the K_D by about a factor of 2
281 while adding a third mutation L10G results in a triple mutant with a $K_D > 500$ μM. Thus, introducing
282 Dpr11-like negative constraints to Dpr10 at these three positions is sufficient to kill binding between
283 Dpr10 and DIP-α. We then carried out a reverse set of experiments aimed at removing negative
284 constraints on Dpr11 to enhance its binding to DIP-α. As can be seen in Figure 3D, the K31V single
285 mutant and the K31V,E29Q double mutant have very little effect, while the triple Dpr11 mutant binds
286 to DIP-α with a K_D of 18.3 μM – weaker than wild-type Dpr10 but still quite strong. Overall, our
287 results indicate that we have successfully identified the negative constraints on the Dpr side of the
288 interface that preclude binding of purple group Dprs to blue group DIPs.
289

b) Negative constraints on the blue subgroup DIP-α that weaken binding to purple subgroup Dprs. FoldX calculations identify positions 6,9,11,15,22 as negative constraints (Figure 4A). We validated a subset of these negative constraints with SPR, positions 9, 15 and 22, and found that all weakened the binding of DIP-γ to Dpr11, although only position 9 had a substantial effect, increasing the K_D of DIP-γ/Dpr11 binding from 7.9 to 37.2 μM (Figure S3A). As can be seen in Figure 4A, there is a charged residue at each of these positions in DIP-γ that forms an ion pair with a complementary charge on purple group Dprs. Each of these positions contains a neutral polar residue in DIP-α which would then disrupt the ion pair and leave an unsatisfied partially buried charge in a hypothetical complex with purple group Dprs.

c) *Negative constraints on blue subgroup Dprs that weaken binding to purple subgroup DIP-γ.* Positions 7,14,16,29,31 on Dpr6 and Dpr10 are predicted to be negative constraints (Figure 4B). Positions 29 and 31 were tested and, as can be seen in the figure, the single K31V mutant increased the K_D of wild-type Dpr11 binding to DIP-γ from 7.9 μM to 22.7 μM while the K31V,E29Q double mutant with two negative constraints had a K_D of 131 μM, almost a factor of 20 greater than wild-type (Figure S3B). The source of the destabilization is evident from the structure figures shows in Figure 4B.

The K to V mutation at position 31 would create a steric clash with Thr at position 11 of DIP-γ and leave two unsatisfied negative charges in the DIP-γ/Dpr11 interface (Asp9 of DIP-γ and Glu25 of Dprs), one of which will also be in a hypothetical complex with blue Dprs (Glu25). The E29Q mutation breaks a salt bridge with Arg6 of DIP-γ leaving an unsatisfied positive charge.

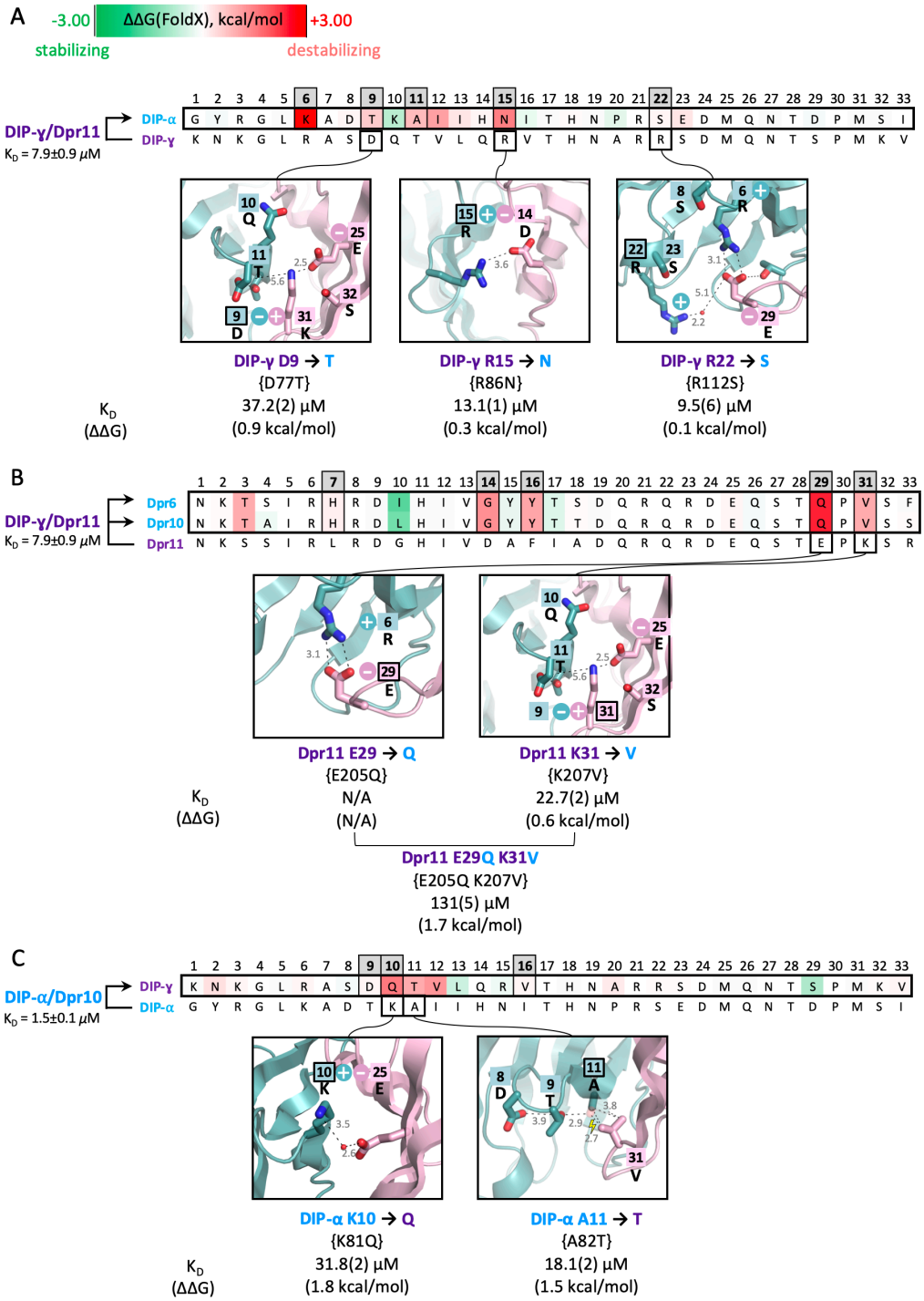

Figure 4. Negative constraints on A) DIP-α, (B), blue Dprs 6/10, (C), DIP-γ that inhibit purple/blue inter-subgroup binding. A) Alignment of interfacial residues of DIP-α and DIP-γ followed by structural details used to explain negative constraint. The average K_D for wild-type DIP-γ/Dpr11 interaction based on five independent experimental measurements is given on the left of the alignment. Experimental K_Ds and ΔΔGs relative to wild type DIP-α/Dpr11 are shown below each insert. All symbols as in Figure 3. B) Alignment of interfacial residues of Dpr6 and Dpr10 with Dpr11. All other details as in 4A. C) Alignment of interfacial residues of DIP-α and DIP-γ. All other details as in 4A. The supporting SPR data for the mutants presented in A, B, and C can be found in Figure S3A, S3B and S3C. For each K_D, the number in parenthesis represents the fitting error in the last significant figure, in μM.

d) Negative constraints on the purple subgroup DIP-γ that weaken binding to blue subgroup Dprs. Three positions (9, 10, 16) in DIP-γ serve as negative constraints based on energy and evolutionary filters (Figure 4C). Position 11 would also be predicted if two of the three template complexes were used in energy filter (Figure S3D). We mutated two of these positions, K10Q and A11T, and tested the extent to which they weaken binding of DIP-α to Dpr10. As seen in Figure S3C, mutations at both of these positions increased the K_D of binding by about an order of magnitude, thus confirming the prediction. Again, the physical basis of the negative constraint is evident from the structure: K10 forms a water-mediated salt-bridge with sequence invariant Glu at position 25 of light blue Dprs that would be disrupted with a neutral Gln; The A to T mutation at position 11 of DIP-γ would introduce a steric clash with Val31 of light blue Dprs.

DIP/Dpr family overview

Figure 5 plots negative constraints identified by FoldX on the surface of hypothetical interfaces that would be formed by a number of non-interacting subgroups. Most of the interface is used to create negative constraints but different regions are exploited by different subgroups (Figure 5). Overall, our predictions implicate 21 positions on the Dpr side of an interface and 17 positions on the DIP side as a source of negative constraints (see positions highlighted in grey, Figure 6). These positions are buried to different degrees in the interface, are located both in loops and secondary structure elements and have different physical-chemical properties (hydrophobic, polar or charged). The majority of the negative constraints reside in loop regions and code for polar or charged residues (21 positions) with 10 positions burying more than 50Å^2 of accessible surface area upon complex formation. Each non-cognate DIP/Dpr subfamily pair was found to be destabilized by a set of about 7 interfacial residues involving both sides of the interface. The physical source of the negative constraint can be shape non-complementarity in the hydrophobic core (Figure 1) (through steric clashes or cavity creation), electrostatic effects (Coulombic repulsion or a desolvation penalty associated with burying unsatisfied charges or polar residues), or both (see examples in Figure 5). Notably, our SPR results suggest that

346 one negative constraint is not sufficient to ablate binding but that at least three are required to assure

347 that members of different subgroups do not form a stable complex.

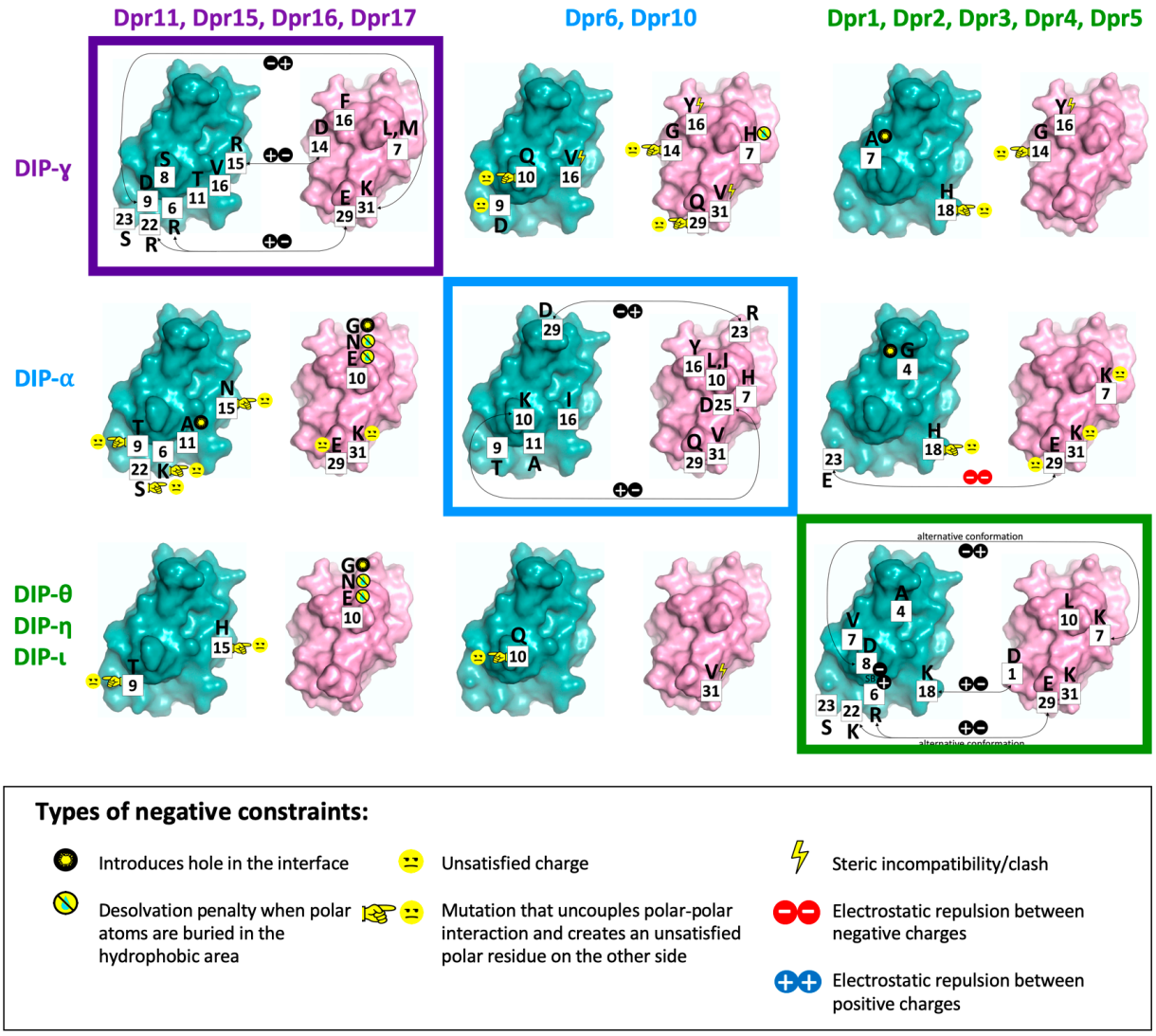

348

349 **Figure 5. Negative constraints in DIP/Dpr non-cognate pairs in *Insecta*.** Predicted negative constraints in three
350 DIP/Dpr subfamilies are shown on the DIP (in cyan) and Dpr (in pink) interacting surfaces of purple, blue, and green
351 subfamilies using an open book representation, with cognate interacting pairs shown enclosed in boxes coded with
352 subfamily color. Family-wide interfacial position number are in filled white boxes. Amino acid residue identity at a
353 negative constraint position is given in a one letter code. The physical origin of each negative constraint is shown with
354 a pictogram as detailed in the enclosed rectangle at bottom.
355

356 Our structure-based predictions of negative constraints include all positions predicted by

357 sequence-based methods, but identify about twice as many positions. Sequence-based methods often

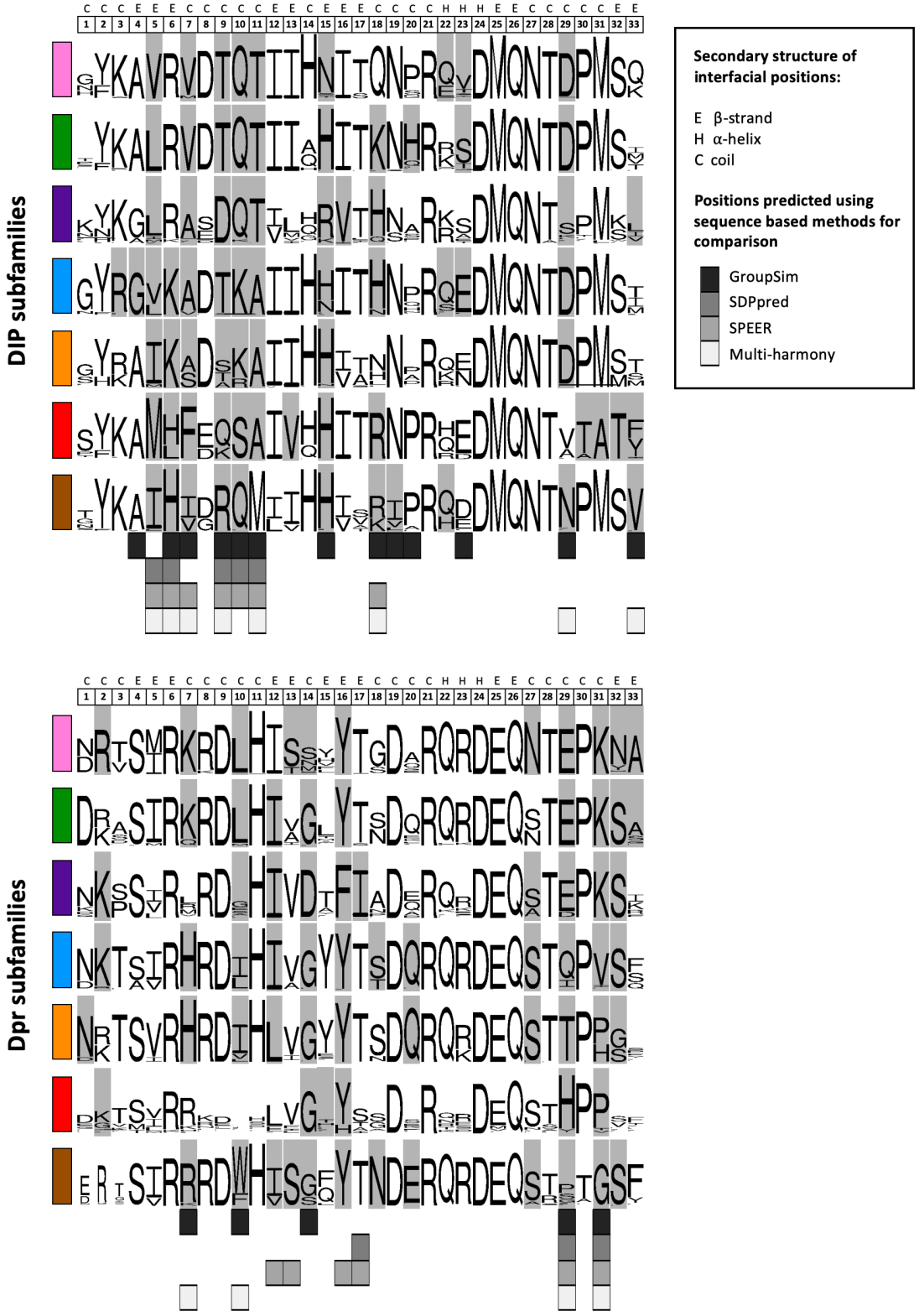

Figure 6. Predicted positions of negative constraints DIP/Dpr subgroups. Logos created for Insecta with residues that function as negative constraints highlighted in grey. Subfamily color-code as in Figure 1B. Each interfacial position (1-33) is annotated above logos with associated secondary structure, as detailed in the boxed legend. Sequence-based predictions of specificity determining positions using sequence-based methods (GroupSim, SDPpred, SPEER, and Multi-Harmony, same as in Figure 2A) are given below logos as specified in boxed inset.

fail to identity positions not fully conserved within a subfamily[22,36]. We also note that the majority of sequence-based methods encounter difficulties in identifying sites that are specific to only one subfamily. For example, positions 14 and 16 correspond to conserved Asp and Phe residues in the purple Dpr subfamily, while other Dprs have Gly and Tyr in these positions, respectively; see Figure 2). Similarly, we predict several residues in the hydrophobic core as potential negative constraints (12, 13, 16 in Dprs and 5, 13, 16 in DIPs), whereas sequence-based methods predict only one of these positions (Figure 2). Of note, these positions were not among those we had experimentally confirmed in this study.

Balancing affinity and specificity

In some interfacial positions, FoldX predicts that mutations to residues found in other subgroups would actually increase affinity (Figures 3 and 4 and Supplemental FoldX data). Some of these suboptimal positions in cognate DIP/Dpr pairs appear to act as negative constraints. As an example, position 10 in purple Dprs, which is either a Gly or a polar residue, is predicted by FoldX to disrupt nonpolar interactions with DIPs in other subgroups. SPR experiments confirmed this prediction (Figure S4); L10G in Dpr10 decreased binding to DIP-α and DIP-β ($\Delta\Delta G$ >1.6 kcal/mol), Notably, G10L increased binding between Dpr11 and DIP-γ by about the same amount, indicating that some cognate binding affinity has been “sacrificed” so as to weaken non-cognate binding.

In a second example, position 7 is predicted to be used by the green Dpr subfamily to weaken non-cognate binding to DIP-α by placing an unsatisfied charge, K7, in non-cognate interfaces (Figure 5). Confirming this prediction, the H7K {H110K} mutation in Dpr6 weakens cognate Dpr6/DIP-α binding by >1.9 kcal/mol[11]. In contrast, the K7H {K82H} mutation in Dpr4 strengthens cognate binding to DIP-η by 0.3 kcal/mol[11], a small effect but within the error bars of our measurements. This is another case where cognate binding is designed to be suboptimal.

Discussion

We have described the structural and energetic origins of the partition of DIPs and Dprs into orthogonal specificity groups defined by SPR-derived binding affinity measurements. We previously analyzed specificity determinants in type II cadherins[5], nectins[8] and DIPs and Dprs[11], primarily through visual inspections of sequences guided by structural data. Here we have adopted a far more extensive and quantitative approach as required by the complexity of the problem we set out to address. Specifically, how specificity is coded on seven subgroups of DIPs and Dprs so that out of the 49 possible subgroup pairings of closely related subfamilies of DIPs and Dprs, only seven form strong pairwise interactions. The problem is complicated by the fact that each subgroup contains between 1 and 5 members on the Dpr side and 1 and 3 members on the DIP side. Asking how 42 combinations of DIP and Dpr subfamilies are designed not to interact, or in some cases to interact weakly, poses a unique set of challenges. Notably, sequence-based methods were able to provide only partial answers to this question.

The approach we have adopted is essentially to build a large set of homology models of complexes that form and do not form and to ask, using FoldX calculations, SPR measurements and visual inspection what is wrong with those that do not form. Since the calculations for each mutation have to be repeated many times so as to obtain proper averages, the findings reported in this paper are based on over 30440 separate FoldX calculations. These led to the identification of 38 negative constraints and to 25 validation tests carried out with SPR. While it is possible of course that some of our predictions are mistaken, the fact that each can be rationalized following visual inspection, that each predicted negative constraint has to be common to all members of a subfamily and be present in orthologous species adds confidence to the validity of our results.

The negative constraints we identified for the most part exploit strong localized unfavorable energetic contributions rather, for example, than more subtle effects that are distributed over many residues (as is the case for type I cadherins where entropic effects involving the movement of entire domains play a role in determining dimerization affinities)[7]. The physical origins of negative

constraints include: replacing a charge in an ion pair with one of opposite sign leading to Coulombic repulsion; replacing one member of an ion pair with a neutral group, which has the effect of burying an unsatisfied charge; mutations in the hydrophobic core to larger amino acids that create steric clashes or to smaller ones that create cavities which lead to packing defects and to weaker hydrophobic contributions to binding. Of course, the same "trick" cannot be reused at the same location for 42 different subgroup pairs. In fact, every set involving negative constraints on DIP and Dpr side of the 42 non-cognate pairs is unique (see supplementary excel file). This is why as discussed above, 38 of 66 interfacial residues, spread over the entire interface needs to be exploited. Notably, in the cases we tested,[11] at least three negative constraints had to be added or removed to essentially switch the specificity of a particular protein from one subgroup to another. As can be seen in Figure 1B, intra-subgroup K_Ds are generally in the range of 10 μM (although some are as weak as 40 μM) while inter-subgroup K_Ds (with a few exceptions) are undetectable, implying a K_D > 500 μM. This suggests that the generation of a new DIP/Dpr specificity requires a change in binding free energy of ~2.5 kcal/mol, a value that is difficult (but not impossible) to reach with one or two mutations.

How is the DIP/Dpr interface designed to achieve affinity and specificity? First, we note that, in common with most cell-cell recognition proteins, DIP/Dpr affinities are in the μM range, a thousand-fold weaker, for example, than many antibody-antigen complexes with substantially smaller binding interfaces. That lower affinities are a general feature of adhesion receptors, even those which are not members of large families, suggest that there are other factors involved that have little to do with negative constraints, for example cellular motility. Moreover, cell-cell avidity involves the interactions of multiple receptors so that there may not be a need to evolve proteins with nanomolar affinities. This may account for the observation above that even cognate interfaces are not optimized for affinity. Moreover, a trade-off between affinity and specificity is to be expected in large protein families with only limited sequence divergence. If an interaction between two family members, say 'a' and 'b', is very strong, then it is more of a challenge, for example, to

generate an isoform 'c' that is similar in sequence to 'b', but interacts very weakly with 'a'. Thus, the higher the specificity requirements, the greater the constraints on absolute affinities.

We find that more than a half of the DIP/Dpr interface (38 of 66 interfacial residues) is utilized for negative constraints across different insect species. However, these only play a role in the context of non-canonical subgroup-subgroup interactions, whereas in any given cognate DIP/Dpr complex, a majority of the interfacial residues likely play a stabilizing role. One can imagine that an ancestral DIP/Dpr complex relied entirely on stabilizing interactions in the hydrophobic core along with additional stabilizing or energy neutral interactions in the periphery. As multiple family members evolved the need for specificity was satisfied through the introduction of negative constraints throughout the interface. This evolutionary strategy is likely used by other large protein families. In addition to manifesting themselves as destabilizing interfacial positions via non-synonymous mutations (as in the case of DIP/Dpr family), negative constraints could potentially be introduced via loop insertions or deletions whose purpose is to avoid undesired interaction, as it was shown in some proteins[37].

Detailed binding affinity measurements have now been reported for a number of families of adhesion receptors. In some cases, for example type II cadherins,[5] the family can be divided into subgroups whose members exhibit considerable promiscuity in their intra-subgroup binding properties while not binding to members of other subgroups. This behavior is reminiscent of the subgroup characteristics of DIPs and Dprs although since there are fewer cadherin specificity groups their evolutionary design is less of a challenge. In both cases binding promiscuity may well be a source of functional redundancy but this has not been established. In contrast, Dscams[1,2] and clustered protocadherins[3,4] are strictly homophilic which, as mentioned above, is an absolute requirement for their role of establishing a unique identity for every neuron. In contrast to DIPs and Dprs, the exquisite specificity of these protein families is established through multi-domain interfaces that allow for a greater degree of fine-tuning. Negative constraints are obviously a central component of their evolutionary design but these have not been characterized in detail yet.

The range of DIP/Dpr binding affinities indicated in Figure 1B raises an additional set of interesting questions regarding the biological role of weak interactions. In a number of cases there is a clearly established connection between molecular affinities and cellular phenotype[8,38] but in general very little is known about this topic. The situation becomes more complex for cells that express more than one family member and/or more than one subgroup member. The ability to design mutants of altered affinities and specificities combined with modern gene editing techniques opens the door to a new type of experiment which probes the molecular basis of cell-cell recognition. We have reported preliminary studies on this problem involving DIP and Dpr mutants, which abolished homophilic or both homophilic and heterophilic interactions in the *Drosophila* retina[11,35]. The next logical step will be to test how subtle changes in affinity and specificity would affect biological phenotype.

Methods

Protein structure alignment

The DIP/Dpr structures used in alignment presented in Figure 1C were, *blue subgroup* - crystal structures of Dpr6/DIP-α (PDBID: 5EO9) and two conformations of Dpr10/DIP-α (PDBID: 6NRQ)[9,10]; *purple subgroup* – crystal structure of Dpr11/DIP-ɣ (PDBID: 6NRR)[10]; *green subgroup* – crystal structures of Dpr4/DIP-η (PDBID: 6EG0) and for two conformations each for Dpr1/DIP-η (PDBID: 6NRW) and Dpr2/DIP-θ (PDBID: 6EG1)[10,11].

Construction of homology models for all superfamily members

We built homology models for each DIP and Dpr Ig1 domain (using the crystal structure of the DIP-η/Dpr4 complex as a template, PDBID: 6EG0). The models are expected in principle to be high quality since there is considerable sequence and structural similarity between intra-family DIP and Dpr Ig1 domains. A few modeled proteins have longer loops than those of the template but these regions do not appear critical for Ig1'-Ig1" interface. Homology models of DIP and Dpr monomers

493 built using MODELLER[39] were superimposed onto Dpr4/DIP-η crystal structures yielding 231
494 DIP/Dpr heterodimers. The side chains of the dimer models were further minimized using the Scwrl4
495 algorithm[40].
496
497 **FoldX protocol to evaluate ΔΔG(binding)**
498 Although FoldX can be used as a "black box" we summarize here the procedures used to
499 calculate ΔΔG(binding). We first refine the structure of a protein complex using the FoldX utility
500 called "RepairPDB" (http://foldxsuite.crg.eu/command/RepairPDB). This procedure "repairs"
501 improbable dihedral angles and van der Waals clashes in a protein. We then run five rounds of
502 "RepairPDB" and confirm that total energy of a protein complex reaches a plateau. The complex
503 whose structure has now been optimized with respect to the FoldX energy function is then used as a
504 starting point for a computational mutagenesis procedure with "BuildModel"
505 (http://foldxsuite.crg.eu/command/BuildModel). A desired mutation is made to the repaired structure
506 and then energy-minimized by sampling rotamers for the mutated residue and its neighboring amino
507 acids. The wild type protein is then energy-minimized with respect to rotamers of the same set of
508 residues. The difference in interaction energy between the mutant and wild type is then calculated
509 between the two protomers in the complex using the 'AnalyseComplex' FoldX utility
510 (http://foldxsuite.crg.eu/command/AnalyseComplex).
511 To test if FoldX achieves convergence for a given mutation we run "BuildModel" ten times by
512 setting the "numberOfRuns" parameter to 10 (http://foldxsuite.crg.eu/parameter/numberOfRuns),
513 which produces ten pairs of wild type and mutant structures, as different neighbors of the mutated
514 residue could be moved during minimization. The average value of the interaction energy obtained
515 via energy decomposition of the total energy using 'AnalyseComplex' defines ΔΔG(binding).
516 Since we carried out 10 separate runs for each FoldX prediction, this yields 30,440 FoldX
517 single point mutation calculations (1 week of computing time on 1 CPU).
518

519 **Calculating the effects of mutations on protein-protein binding**

520 The following is a summary of the methods evaluated for the calculation of the effects of mutations
521 on binding free energies. ***FoldX*** evaluates the effects of mutations using an empirical force-field that
522 allows side chains to move but keeps the backbone rigid[18,31]; ***mCSM*** is a machine learning method
523 based on the assumption that the impact of a mutation is correlated with atomic-distance patterns in
524 surrounding amino acids[30]; ***BeAtMusic*** relies on a set of coarse-grained statistical potentials derived
525 from known protein structures[27]. BeAtMusic is the fastest of all the methods we tested – it takes
526 seconds to assess all possible mutations in a protein chain or at the interface; ***MutaBind*** utilizes a
527 combination of molecular mechanics force fields, statistical potentials and a fast side-chain
528 optimization algorithm; ***Rosetta flex ddG***[24] samples conformational diversity using "backrub" to
529 generate an ensemble of models and then applies torsional minimization, side-chain repacking, and
530 averaging across this ensemble to calculate $\Delta\Delta G$; ***BindProfX***[32] combines a sequence profile
531 conservation score of structural homologues with the FoldX potential. Data on the performance of
532 these methods is summarized in Table S2.
533
534
535 **Sequence-logo preparation**
536 To get orthologs of DIPs and Dprs in Insecta species we performed the search using reciprocal best
537 hit BLAST[41] with an e-value cutoff of 10^{-35} using in-house developed scripts on non-redundant
538 BLAST database. The resulting 2950 Dpr sequences and 2005 DIP sequences (121 species) were
539 screened using CD-HIT[42] with 100% threshold to get rid of redundancy arising from multiple GI
540 (GenInfo Identifier) numbers pointing to the same protein product. The obtained non-redundant set
541 of full-length sequences corresponding to DIP(*i*) or Dpr(*j*) was combined with a reference sequence
542 (DIP-α or Dpr6 respectively), and aligned using Clustal-Omega[43]. The multiple sequence alignments
543 (MSA) of each DIP(i) and Dpr(j) were further processed to remove sequences that had non-complete
544 Ig1 domains and to extract interfacial positions based on the reference sequences. Sequence

545 logos[44] based on the MSAs presented in Figure 2 were created separately for each *Drosophila* DIP
546 and Dpr based on 2570 Dpr and 1732 DIP sequences. Sequence logos were also prepared on a
547 subfamily level by combining sequences of all its members, see Figure 6.
548
549 **Sequence-based methods used to predict specificity residues**
550 GroupSim[20] analyzes evolutionary conservation patterns using physico-chemical properties of amino
551 acids by means of similarity matrices; SDPpred[21] uses information theory schemes based on
552 Shannon entropy and frequency scores; SPEER[22] uses amino acid properties, entropy and
553 evolutionary rates by analyzing quantitative measures of the conservation patterns of protein sites
554 based on their physico-chemical properties and the heterogeneity of evolutionary changes between
555 and within the protein subfamilies. Multi-Harmony[23] uses a combination of Shannon entropy and
556 machine learning.
557 All the sequence-based methods we use for determination of specificity positions require
558 predefined subgrouping of sequences based on their binding preferences. We grouped the above
559 2570 Dpr and 1732 DIP sequences (truncated to 33 interfacial residues only) into seven sets (DIP-
560 θ/η/ι/, DIP-κ, DIP-α, DIP-β/λ, DIP-γ, DIP-δ, DIP-ε,ζ for DIPs, and Dpr1/2/3/4/5, Dpr7, Dpr6/10,
561 Dpr8/9/21, Dpr11/15/16/17, Dpr12, Dpr13,14,18,19,20 for Dprs).
562 We rely on the assumption that orthologs in the same subfamily conserve their interaction
563 specificity. This assumption would not work for comparison of proteins in species that are too far
564 away from each other on the tree of life, but since we consider orthologs within one class, *Insecta*,
565 the assumption is likely to be correct. To justify this, we calculated the pairwise sequence identities
566 within *Insecta* orthologs for each DIP and Dpr, and the intra-subgroup pairwise sequence identity for
567 each DIP and Dpr *Insecta* subgroup (~78%) using multiple sequence alignments of interfacial
568 residues. These values are comparable to intra-subgroup pairwise sequence identities of interfacial
569 residues in *Drosophila Melanogaster* (~80%) and are consistently higher that inter-subgroup
570 pairwise sequence identities in *Drosophila Melanogaster* or *Insecta* (~50%). Only one subfamily (red

Dpr) is an exception to the rule - it has relatively low conservation in *Insecta* (48%), but it is as diverse within the group in *Drosophila Melanogaster* (40%).

Protocol for identifying negative constraints.

Energy filter

Positions were filtered based on FoldX calculations of *Drosophila Melanogaster* DIP/Dpr complexes. If positions were predicted to cause destabilizing effects ($\Delta\Delta G$ >=0.05 kcal/mol) for every DIP or Dpr fly subgroup member in the context of binding to a member of another Dpr or DIP subgroup, the position were accepted provided $\Delta\Delta G$ >=0.05 kcal/mol for every subfamily template complex used in the FoldX calculations. The cutoff value for $\Delta\Delta G$ was chosen based on estimated standard deviation value for mutating an interfacial amino acid into self ($\Delta\Delta G = 0.00 \pm 0.05$ kcal/mol). Positions that passed energy filter were further subject to the evolutionary filter.

Evolutionary filter

Positions were filtered using multiple sequence alignments (MSAs) for DIP and Dpr subfamilies based on sequences of insect orthologs (see above how these were obtained). For every non-cognate DIP(i)/Dpr(j) family, to filter positions on DIP side we compared corresponding positions from DIP(i) and DIP(j) subfamilies in MSAs. To filter positions on Dpr side we compared positions from Dpr(i) and Dpr(j) subfamilies in MSAs. The position was accepted if at least one of the three conditions outlined below was true.

1) If positions in "i" and "j" subgroup were both conserved (S<0.23) and different in identity – the position was accepted (if purifying selection imposed evolutionary pressure to preserve a certain type of an amino acid, even differences in shape/size of similar amino acids (L and I, or R and K, might be of significance). Here S stands for Shannon entropy as the measure of conservation. It's calculated using the following formula $\boldsymbol{S} = -\sum_{i=1}^{N} \boldsymbol{f_i log_{21} f_i}$ where f_i is the fraction (frequency of occurrence) of residues of amino acid type present at a position in

MSA and N is the number of amino acid types (base of 21 was picked to account for 20 amino acids types and a gap).

2) If positions in "i" and "j" subgroup had difference in biophysical property (to account for negative constraints associated with either desolvation penalty or electrostatic repulsion). We binned 20 amino acids into four property groups: hydrophobic (I, V, L, M, F, W, A, C, G, P), polar (S,T,Q,N,H,Y), positively charged (K,R), and negatively charged (E,D). Then we summed up the instances where amino acids at a position of subfamily "i" (aa_i) were different in biophysical property from aa_j weighted by the occurrences of aa_i and aa_j in MSAs ($\sum_{i=1}^{N} f_{aa_i} \sum_{j=1}^{M} f_{aa_j} \times 100\%$). The positions were accepted if there was >90% difference in biophysical property between two positions.

3) If positions in "i" and "j" subgroup had differences in size (amino acids of one subgroup always bigger, or always smaller in size than those appearing in the other subgroup to justify negative constraint involving steric clashes or introducing holes in the interfaces, respectively). We binned 20 amino acids into five size groups, which were based on the volume of amino acids: tiny (G, A, S), small (C, D, P, N, T), medium (E, V, Q, H), large (M, I, L, K, R), bulky (F, Y, W). The percent difference was weighted by amino acid occurrences (in the same manner as above) and the positions were accepted at >90% cutoff.

Plasmid construction and protein expression

All proteins were produced by expression in human embryonic kidney cells (HEK293F). DNA sequences encoding DIP and Dpr extracellular regions were amplified by PCR and sub-cloned into the mammalian expression vector VRC-8400[45] between the NotI and BamHI sites. Sequence boundaries for each DIP and Dpr were the same as those defined in Cosmanescu et al.[11] All sequences were preceded by the signal sequence of human binding immunoglobulin protein BiP (MKLSLVAAMLLLLSAARA), and a kozak sequence (GCCACC). Constructs were followed by a C-terminal hexa-histidine tag. Point mutations were introduced using the QuickChange method (Agilent). HEK293F cells were transiently transfected with each expression construct using the

polyethylenimine method[46], and cells were expanded and grown in shake flasks in a CO2 incubator for 3-6 days.

Protein purification

Conditioned media was equilibrated to 10mM Tris-HCl pH 8.0, 500mM NaCl, 3mM $CaCl_2$ and 5mM Imidazole pH 8.0 and incubated with Ni^{2+} charged IMAC Sepharose 6 Fast Flow resin (GE Healthcare) for 1 hr at 25°C. Resin was washed with at least 20 column volumes of buffer containing 10mM Imidazole pH 8.0. SDS gel electrophoresis was used to detect which elution fractions contained the desired protein.

Proteins were further purified by size-exclusion chromatography (Superdex 200 HiLoad 26/60 or Superdex S200 Increase 10/300 GL; GE Healthcare) on an AKTA pure fast protein liquid chromatography system (GE Healthcare). Most proteins were stored in a buffer of 10mM Bis-Tris pH 6.6 and 150mM NaCl. UV absorbance at 280nm was used to determine protein concentration and verification of purity was determined by gel electrophoresis. Accurate molecular weights were determined through MALDI-TOF mass spectrometry at the Proteomics Shared Resource facility at Columbia University.

Sedimentation equilibrium by analytical ultracentrifugation

Experiments were performed in a Beckman XL-A/I analytical ultracentrifuge (Beckman-Coulter, Palo Alto CA, USA), utilizing six-cell centerpieces with straight walls, 12 mm path length and sapphire windows. Protein samples were dialyzed to 10mM Bis-Tris pH 6.6, 150mM NaCl. The samples were diluted to an absorbance of 0.65, 0.43 and 0.23 at a 10 mm path length and 280 nm wavelength in channels A, B and C, respectively. Dilution buffer were used as blank. The samples were run at four speeds. Most proteins were run at 15000, 19000, 23000, and 27000 RPM. For all runs the lowest speed was held for 20hr and then four scans were taken with a 1hr interval, the second lowest held for 10hr then four scans with a 1hr interval, and the third lowest and highest speed measured as the

second lowest speed. Measurements were done at 25°C, and detection was by UV at 280 nm. Solvent density and protein v-bar were determined using the program SednTerp. (Alliance Protein Laboratories) To calculate the K_D and apparent molecular weight, data were fit to a global fit model, using HeteroAnalysis software package, obtained from University of Connecticut[47] (http://www.biotech.uconn.edu/auf).

Surface Plasmon Resonance (SPR) binding experiments

SPR binding assays were performed using a Biacore T100 biosensor equipped with a Series S CM4 sensor chip. To minimize artificial binding resulting from enhanced- avidity effects of oligomers interacting with an immobilized ligand, DIPs and their respective mutants, were consistently used as ligands rather than analytes, and immobilized over independent flow cells using amine-coupling chemistry in HBS pH 7.4 (10mM HEPES, 150mM NaCl) buffer at 25°C using a flow rate of 20 µL/min. Dextran surfaces were activated for 7 minutes using equal volumes of 0.1M NHS(N-Hydroxysuccinimide) and 0.4M EDC(1-Ethyl-3-(3-dimethylaminopropyl)carbodiimide). Each protein of interest was immobilized at ~30µg/mL in 10 mM sodium acetate, pH 5.5 until the desired immobilization level was achieved. The immobilized surface was blocked using a 4-minute injection of 1.0 M ethanolamine, pH 8.5. Typical immobilization levels ranged between 760-980 RU. To minimize nonspecific binding the reference flow cell was blocked by immobilizing BSA in 10 mM sodium acetate, pH 4.25 for 3 minutes using a similar amine-coupling protocol as described above. For each experiment where DIP mutants were immobilized to the chip surface, the wild type molecule was immobilized on an adjacent flow cell as a positive control.

Binding analysis was performed at 25°C in a running buffer of 10 mM Tris-HCl, pH 7.2, 150mM NaCl, 1mM EDTA, 1 mg/mL BSA and 0.01% (v/v) Tween-20. Analytes were prepared in running buffer and tested at nine concentrations using a three-fold dilution series ranging from 81 to 0.012 µM for data shown in Figure 3C and D, Figure S3A-C, Figure S4, with the of exception Dpr10 binding to DIP-α A11T in Figure S3C, which was tested at nine concentration ranging from 27 to 0.004 µM, prepared

673 in a three-fold dilution series. Dpr6 was tested at eight concentrations ranging from 9 to 0.004 μM,
674 prepared in a running buffer using a three- fold dilution series for data presented in Figure S1A, with
675 the exception of experiments over the DIP-α I16A and DIP-α K10Q G4S surfaces where Dpr6 was
676 used at ten concentrations ranging from 81-0.004 μM, using a three-fold dilution series. Dpr10 binding
677 experiments in Figure S1B, was tested at nine concentrations ranging from 27 to 0.004 μM, prepared
678 in a running buffer using a three- fold dilution series, with the exception of experiments over surfaces
679 immobilized with DIP-α I16A, K10Q G4S and K10Q D29S where the analyte was used at ten
680 concentrations ranging from 81-0.004 μM, using a three-fold dilution series. In each experiment, every
681 concentration was tested in duplicate. Within each experiment, there two technical replicates starting
682 with a single concentration series, where samples are tested in order of increasing concentration,
683 followed by a repeat of the same concentration series, performed again from low to high concentration.
684 During a binding cycle, the association phase between each analyte and the immobilized molecule
685 was monitored for either 30 or 40 seconds as indicated by the plotted sensorgrams, followed by 120-
686 second dissociation phase, each at 50 μL/min. At the end of the dissociation phase the signal returned
687 to baseline thus eliminating the need for a regeneration step. The last step was buffer wash injection
688 at 100 μL/min for 60 seconds. The analyte was replaced by buffer every two or three binding cycles
689 to double-reference the binding signals by removing systematic noise and instrument drift. The
690 duplicate binding responses were fit globally, using an 1:1 interaction model and a single K_D was
691 calculated as the analyte concentration that would yield 0.5 R_{max}[48] and a fitting error. In cases where
692 the highest analyte concentration is only around the K_D, we use the R_{max} value for a saturating binding
693 isotherm shown on the same plot, as a global R_{max}, to fit the binding isotherms for weaker interactions
694 and calculate a K_D. The data was processed using Scrubber 2.0 (BioLogic Software).
695 For several wild type interactions discussed in this manuscript, Dpr10/DIP-α, Dpr6/DIP-α, and
696 Dpr11/DIP-γ, we have also determined K_Ds from independent experiments. For the Dpr10/DIP-α
697 binding pair, the K_D from six independent experiments is 1.5±0.1 μM, and similarly for the Dpr6/DIP-
698 α, the K_D from six independent experiments is 2.0±0.2 μM. The K_D from five independent

699 experiments for Dpr11/DIP-γ is 7.9±0.9μM. The standard deviation in ΔΔG values computed based
700 on K_D measurements of the above three cases do not exceed 0.1 kcal/mol. Therefore, mutations
701 resulting in ΔΔG (SPR) > | 0.2 kcal/mol | are likely to be significant.
702 In a note added in proof, Cheng et al.[10] recently criticized K_Ds we previously determined via SPR
703 experiments[11], specifically for the interacting pairs Dpr6/DIP-α, Dpr11/DIP-γ and Dpr1/DIP-η, for
704 being consistently weaker than K_Ds they reported. The following discussion explains how differences
705 in experimental methodology likely explains these differences and raises issues about the approach
706 used by Cheng et al.[10]. The underlying challenge in both sets of measurements is that some DIPs
707 homodimerize, a problem that is discussed by Rich and Myszka in their 2006 review of SPR data[49].
708 We addressed this problem by immobilizing DIP proteins to the chip surface, using Dprs as analytes,
709 to minimize artificially lower K_Ds resulting from homodimers used as analytes. It has been suggested
710 that an alternate "fix" is to use the free monomer analyte concentration in K_D calculations[10].
711 However, the monomer/dimer equilibrium in the analyte can shift the moment the analyte is injected
712 over a surface immobilized with a heterophilic binding partner, which changes the monomeric
713 analyte concentration available for a heterophilic binding reaction over the course of the experiment.
714 Therefore, this correction does not adequately solve the problem.
715 Moreover, to calculate the free monomer analyte concentration of DIP-η, Cheng et al. used size
716 exclusion chromatography and SPR to calculate a homophilic K_D of 23 μM and 14 μM,
717 respectively,[10] compared to our analytical ultracentrifugation-determined K_D of 56.2 μM[11]. Given the
718 reliability of AUC measurements, this highlights the problems associated with Chang et al.'s
719 approach. Most importantly these numbers suggest that the differences in K_D reported in both
720 studies are due in part to the use of different biophysical techniques used to study these molecules.
721 In addition, for many of the results that differ between our studies and Cheng et al.[10], these authors
722 relied on ECIA experiments with artificially multimerized molecules. As previously discussed in detail
723 in Cosmanescu et al.[11] although ECIA can be used to detect interactions in a high-throughput
724 fashion and without the need for purified proteins, it involves the use of multimerized forms of both

the prey and the bait molecules, and thus introduces artificial avidity to amplify binding signals, enhancing the likelihood of positive detection, but masking the real binding affinities between interactants. In addition, the use of unpurified protein supernatants[10] could introduce experimental bias toward identifying interactions between molecules that are more easily expressed at higher levels compared to proteins that can be difficult to express.

Acknowledgments

This work was supported by US National Science Foundation grant MCB-1412472 (to B.H.) and NIH grant R01 MH114817 (to L.S.). B.H. is Investigator of the Howard Hughes Medical Institute. We thank Engin Ozkan for providing DIP-α/Dpr10 and DIP-γ/Dpr11 structures and density maps prior to their appearance in the PDB database.

Author Contributions

A.P.S., L.S. and B.H. conceived the project, designed experiments, and analyzed data. A.P.S. carried out all the theoretical and computational work. P.S.K. performed and analyzed SPR experiments. G.A. performed AUC experiments. J.J.B, F.C., S.M. produced expression vectors and proteins. A.P.S. and F.C. designed mutant constructs. A.P.S., B.H., and L.S. wrote the manuscript.

Data and code availability

The raw data that support the findings of this study, and the code used to generate it, are available from the corresponding authors upon request.

References

1. Zipursky, S.L., Wojtowicz, W.M. & Hattori, D. Got diversity? Wiring the fly brain with Dscam. *Trends Biochem Sci* **31**, 581-8 (2006).

2. Wojtowicz, W.M. et al. A vast repertoire of Dscam binding specificities arises from modular interactions of variable Ig domains. *Cell* **130**, 1134-45 (2007).
3. Thu, C.A. et al. Single-cell identity generated by combinatorial homophilic interactions between alpha, beta, and gamma protocadherins. *Cell* **158**, 1045-1059 (2014).
4. Schreiner, D. & Weiner, J.A. Combinatorial homophilic interaction between gamma-protocadherin multimers greatly expands the molecular diversity of cell adhesion. *Proc Natl Acad Sci U S A* **107**, 14893-8 (2010).
5. Brasch, J. et al. Homophilic and Heterophilic Interactions of Type II Cadherins Identify Specificity Groups Underlying Cell-Adhesive Behavior. *Cell Rep* **23**, 1840-1852 (2018).
6. Katsamba, P. et al. Linking molecular affinity and cellular specificity in cadherin-mediated adhesion. *Proc Natl Acad Sci U S A* **106**, 11594-9 (2009).
7. Vendome, J. et al. Structural and energetic determinants of adhesive binding specificity in type I cadherins. *Proc Natl Acad Sci U S A* **111**, E4175-84 (2014).
8. Harrison, O.J. et al. Nectin ectodomain structures reveal a canonical adhesive interface. *Nat Struct Mol Biol* **19**, 906-15 (2012).
9. Carrillo, R.A. et al. Control of Synaptic Connectivity by a Network of Drosophila IgSF Cell Surface Proteins. *Cell* **163**, 1770-1782 (2015).
10. Cheng, S. et al. Molecular basis of synaptic specificity by immunoglobulin superfamily receptors in Drosophila. *Elife* **8**(2019).
11. Cosmanescu, F. et al. Neuron-Subtype-Specific Expression, Interaction Affinities, and Specificity Determinants of DIP/Dpr Cell Recognition Proteins. *Neuron* (2018).
12. Tan, L. et al. Ig Superfamily Ligand and Receptor Pairs Expressed in Synaptic Partners in Drosophila. *Cell* **163**, 1756-69 (2015).
13. Ozkan, E. et al. An extracellular interactome of immunoglobulin and LRR proteins reveals receptor-ligand networks. *Cell* **154**, 228-39 (2013).
14. Havranek, J.J. & Harbury, P.B. Automated design of specificity in molecular recognition. *Nat Struct Biol* **10**, 45-52 (2003).
15. Humphris, E.L. & Kortemme, T. Design of multi-specificity in protein interfaces. *PLoS Comput Biol* **3**, e164 (2007).
16. Leaver-Fay, A. et al. Computationally Designed Bispecific Antibodies using Negative State Repertoires. *Structure* **24**, 641-651 (2016).
17. Mandell, D.J. & Kortemme, T. Computer-aided design of functional protein interactions. *Nat Chem Biol* **5**, 797-807 (2009).
18. Schymkowitz, J. et al. The FoldX web server: an online force field. *Nucleic Acids Res* **33**, W382-8 (2005).
19. Grigoryan, G., Reinke, A.W. & Keating, A.E. Design of protein-interaction specificity gives selective bZIP-binding peptides. *Nature* **458**, 859-64 (2009).
20. Capra, J.A. & Singh, M. Characterization and prediction of residues determining protein functional specificity. *Bioinformatics* **24**, 1473-80 (2008).
21. Kalinina, O.V., Mironov, A.A., Gelfand, M.S. & Rakhmaninova, A.B. Automated selection of positions determining functional specificity of proteins by comparative analysis of orthologous groups in protein families. *Protein Sci* **13**, 443-56 (2004).
22. Chakrabarti, S., Bryant, S.H. & Panchenko, A.R. Functional specificity lies within the properties and evolutionary changes of amino acids. *J Mol Biol* **373**, 801-10 (2007).

23. Brandt, B.W., Feenstra, K.A. & Heringa, J. Multi-Harmony: detecting functional specificity from sequence alignment. *Nucleic Acids Res* **38**, W35-40 (2010).
24. Barlow, K.A. et al. Flex ddG: Rosetta Ensemble-Based Estimation of Changes in Protein-Protein Binding Affinity upon Mutation. *J Phys Chem B* **122**, 5389-5399 (2018).
25. Buss, O., Rudat, J. & Ochsenreither, K. FoldX as Protein Engineering Tool: Better Than Random Based Approaches? *Comput Struct Biotechnol J* **16**, 25-33 (2018).
26. Choi, Y., Furlon, J.M., Amos, R.B., Griswold, K.E. & Bailey-Kellogg, C. DisruPPI: structure-based computational redesign algorithm for protein binding disruption. *Bioinformatics* **34**, i245-i253 (2018).
27. Dehouck, Y., Kwasigroch, J.M., Rooman, M. & Gilis, D. BeAtMuSiC: Prediction of changes in protein-protein binding affinity on mutations. *Nucleic Acids Res* **41**, W333-9 (2013).
28. Geng, C., Vangone, A., Folkers, G.E., Xue, L.C. & Bonvin, A. iSEE: Interface structure, evolution, and energy-based machine learning predictor of binding affinity changes upon mutations. *Proteins* (2018).
29. Li, M., Simonetti, F.L., Goncearenco, A. & Panchenko, A.R. MutaBind estimates and interprets the effects of sequence variants on protein-protein interactions. *Nucleic Acids Res* **44**, W494-501 (2016).
30. Pires, D.E., Ascher, D.B. & Blundell, T.L. mCSM: predicting the effects of mutations in proteins using graph-based signatures. *Bioinformatics* **30**, 335-42 (2014).
31. Guerois, R., Nielsen, J.E. & Serrano, L. Predicting changes in the stability of proteins and protein complexes: a study of more than 1000 mutations. *J Mol Biol* **320**, 369-87 (2002).
32. Xiong, P., Zhang, C., Zheng, W. & Zhang, Y. BindProfX: Assessing Mutation-Induced Binding Affinity Change by Protein Interface Profiles with Pseudo-Counts. *J Mol Biol* **429**, 426-434 (2017).
33. Ashley, J. et al. Transsynaptic interactions between IgSF proteins DIP-α and Dpr10 are required for motor neuron targeting specificity in Drosophila. *bioRxiv* (2018).
34. Venkatasubramanian, L. et al. Stereotyped Terminal Axon Branching of Leg Motor Neurons Mediated by IgSF Proteins DIP-α and Dpr10. *bioRxiv* (2018).
35. Xu, S. et al. Interactions between the Ig-Superfamily Proteins DIP-alpha and Dpr6/10 Regulate Assembly of Neural Circuits. *Neuron* (2018).
36. Chakraborty, A. & Chakrabarti, S. A survey on prediction of specificity-determining sites in proteins. *Brief Bioinform* **16**, 71-88 (2015).
37. Akiva, E., Itzhaki, Z. & Margalit, H. Built-in loops allow versatility in domain-domain interactions: lessons from self-interacting domains. *Proc Natl Acad Sci U S A* **105**, 13292-7 (2008).
38. Togashi, H. et al. Nectins establish a checkerboard-like cellular pattern in the auditory epithelium. *Science* **333**, 1144-7 (2011).
39. Eswar, N. et al. Comparative protein structure modeling using Modeller. *Curr Protoc Bioinformatics* **Chapter 5**, Unit-5 6 (2006).
40. Krivov, G.G., Shapovalov, M.V. & Dunbrack, R.L., Jr. Improved prediction of protein side-chain conformations with SCWRL4. *Proteins* **77**, 778-95 (2009).
41. Altschul, S.F., Gish, W., Miller, W., Myers, E.W. & Lipman, D.J. Basic local alignment search tool. *J Mol Biol* **215**, 403-10 (1990).

838 42. Fu, L., Niu, B., Zhu, Z., Wu, S. & Li, W. CD-HIT: accelerated for clustering the next-
839 generation sequencing data. *Bioinformatics* **28**, 3150-2 (2012).
840 43. Sievers, F. et al. Fast, scalable generation of high-quality protein multiple sequence
841 alignments using Clustal Omega. *Mol Syst Biol* **7**, 539 (2011).
842 44. Crooks, G.E., Hon, G., Chandonia, J.M. & Brenner, S.E. WebLogo: a sequence logo
843 generator. *Genome Res* **14**, 1188-90 (2004).
844 45. Barouch, D.H. et al. A human T-cell leukemia virus type 1 regulatory element enhances
845 the immunogenicity of human immunodeficiency virus type 1 DNA vaccines in mice and
846 nonhuman primates. *J Virol* **79**, 8828-34 (2005).
847 46. Baldi, L., Hacker, D.L., Meerschman, C. & Wurm, F.M. Large-scale transfection of
848 mammalian cells. *Methods Mol Biol* **801**, 13-26 (2012).
849 47. Cole, J.L., Lary, J.W., T, P.M. & Laue, T.M. Analytical ultracentrifugation: sedimentation
850 velocity and sedimentation equilibrium. *Methods Cell Biol* **84**, 143-79 (2008).
851 48. Rich, R.L., Myszka, D.G. Extracting affinity constants from biosensor binding responses.
852 in *Label-free biosensors : techniques and applications* (ed. Cooper, M.A.) pp. 48-84
853 (Cambridge; New York: Cambridge University Press, 2009).
854 49. Rich, R.L. & Myszka, D.G. Survey of the year 2006 commercial optical biosensor
855 literature. *J Mol Recognit* **20**, 300-66 (2007).
856